Unique Reaction Path in Heterogeneous Catalysis: The Concerted Semi-Hydrogenation of Propyne to Propene on CeO_2

Max García-Melchor,* Luca Bellarosa, and Núria López

Institute of Chemical Research of Catalonia (ICIQ), Av. Països Catalans, 16, E-43007 Tarragona, Spain

Supporting Information

ABSTRACT: Despite its ubiquity in homogeneous and enzymatic catalysis, concerted mechanisms have been overlooked for heterogeneously catalyzed reactions. The elusive nature of transition states leaves Density Functional Theory, DFT, as the only robust tool for their identification and characterization. By means of this method, we show that a concerted path takes part in the recently discovered semi-hydrogenation of propyne on CeO_2, for which an excellent activity and selectivity have been reported. The high surface H coverage imposed by the experimental hydrogenation conditions induces site isolation and drives the reaction through a six-membered ring transition state. This unprecedented pathway accounts for many of the experimental observations, such as the unique *syn*-stereoselectivity, the excellent alkene selectivities, or the high temperature and large H_2/alkyne ratios required.

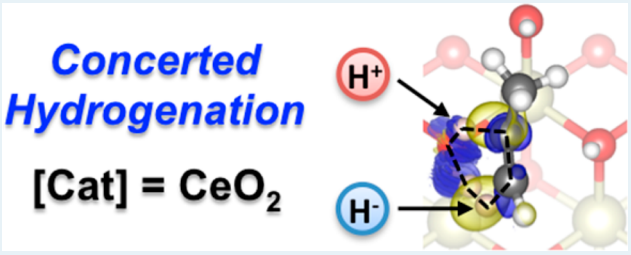

KEYWORDS: *hydrogenation, CeO_2, H_2 activation, DFT, reaction mechanisms, alkynes, olefins, concerted*

1. INTRODUCTION

The reaction mechanisms that operate in metal-based heterogeneous catalysis imply the coordination of reactants to the metal surface followed by elementary steps consisting in single atom-by-atom transfers (forming/breaking only one bond).[1,2] This is at odds with gas-phase, homogeneous, and enzymatic catalysis, where concerted mechanisms involving the addition of more than one atom at a time are ubiquitous. In the present work, we show that these paths are not forbidden in heterogeneous reactions, but rather, they require specific catalytic environments and surface ensembles to come out. For this study, we have focused on one of the most relevant reactions in heterogeneous catalysis: the partial hydrogenation of alkynes shown in eq 1.

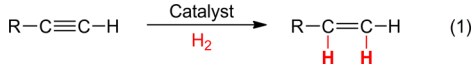

(1)

Over the last decades, alkyne semihydrogenation has attracted great attention due to its primary role in the purification of rich olefin streams in oil refineries and its potential for the large scale production of commodity chemicals.[3,4] This reaction is traditionally carried out by different formulations of Pd catalysts,[5−7] though it can also take place with poorer activities on other active metals[8] or on Au[9] and Ag[10] nanoparticles. The added advantage of Pd-based catalysts is that they provide high activities at moderate temperatures and hydrogen pressures; however, they suffer from selectivity losses, namely, overhydrogenation and oligomerization reactions.[4,9] To overcome this issue, numerous experimental and theoretical works have analyzed factors that affect the selectivity of catalysts, including particle size,[6] the presence of subsurface species,[11−15] and the addition of modifiers or promoters.[16−18] At the same time, the replacement of noble metals with more economical substitutes has been also a subject of intensive research.[19,20]

Very recently, ceria has been proven to catalyze the partial hydrogenation of alkynes with excellent selectivities, between 71 and 91%, at high degrees of conversion.[21,22] The optimal reaction conditions for this new catalytic system require a relatively high temperature (T = 523 K) and a large H_2/alkyne ratio (30:1), which has been attributed to the inherent difficulty of CeO_2 in activating H_2.[21−23] This unprecedented activity of a metal oxide in hydrogenation, coupled with the fact that reaction mechanisms on these materials might divert from those on metals[24] due to their acid−base properties,[25] opens new scenarios for the activation of selected bonds.

The quintessential hydrogenation mechanism involving metal surfaces is the *Horiuti−Polanyi* or *dissociative mechanism* (Scheme 1), which was proposed in 1934.[26] It entails the homolytic dissociation of H_2 on the catalyst surface followed by the sequential addition of H atoms to the adsorbed alkyne. This mechanism operates not only on regular surfaces of active metals like Pd[27] or Ni[28] but also on low-coordinated sites of the less active Au nanoparticles.[29] Alternatively, for catalysts that are not able to break H_2, the *associative mechanism* depicted in Scheme 1 sets in. In this case, the H−H bond is directly activated by the adsorbed alkyne and the metal surface, which

Scheme 1. Possible Reaction Mechanisms for the Partial Hydrogenation of Alkynes in Heterogeneous Processes

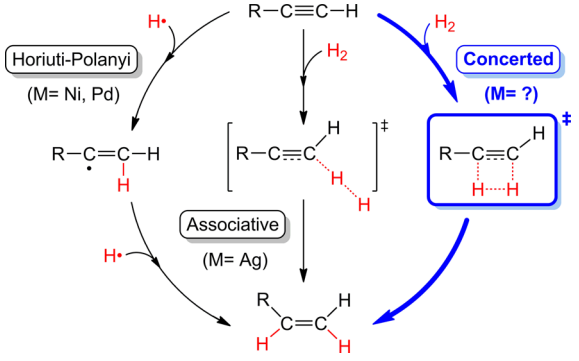

results in the incorporation of a H atom to these two fragments. Subsequently, the surface H is directly transferred to the alkyne yielding the desired olefin. An example of this associative mechanism is the recently reported propyne to propene conversion on Ag nanoparticles.[10]

A third hydrogenation mechanism, for which there is no experimental or computational evidence to date, consists in the simultaneous addition of two H atoms to the adsorbed alkyne. This concerted mechanism (Scheme 1) resembles both the acid−base-like mechanism involved in the hydroboration of double and triple carbon bonds,[30] and the one in pericyclic reactions.[31] Thus, its operation under certain reaction conditions cannot be ruled out.

Herein, we present a thorough mechanistic study on the recently discovered semihydrogenation of propyne catalyzed by CeO_2.[21] We found that the surface coverage under the experimental hydrogenation conditions drives the reaction toward the concerted path highlighted in the blue square of Scheme 1. This unprecedented mechanism accounts for many of the experimental observations, such as the unique *syn*-stereoselectivity, the excellent alkene selectivities, or the high temperature and large H_2/alkyne ratios required,[21] and furthermore, the mechanism may provide insight on the structure sensitivity recently observed.[32]

2. COMPUTATIONAL METHODS

The reaction mechanism for the CeO_2-catalyzed semihydrogenation of propyne under relevant experimental conditions were investigated by means of DFT as implemented in the VASP code, version 5.3.2.[33,34] In all the calculations, the core electrons of Ce, C, and O atoms were replaced by projector-augmented wave potentials,[35] whereas their valence electrons were expanded in plane waves with a kinetic energy cutoff of 500 eV. In order to describe the strongly correlated character of the Ce-4f orbitals correctly, a Hubbard *U*-like term was added to the Perdew−Burke−Ernzenhof functional.[36] This was carried out following the DFT+*U* approach of Dudarev et al.,[37] which defines the difference between the Coulomb and exchange energy terms as the effective *U* parameter, U_{eff}. This parameter was set to 4.5 eV, as proposed by Fabris et al.[38]

The optimized lattice parameter of ceria using a Γ-centered 7 × 7 × 7 k-point grid was a_{calc} = 5.497 Å, which is in good agreement with the experimental value of a_{exp} = 5.411 Å.[39] The CeO_2 catalyst was modeled as slabs containing nine atomic layers of the most exposed (111) facet and a vacuum space of at least 10 Å. The atoms in $p(2 \times 2)$ supercells were optimized using a Γ-centered 3 × 3 × 1 k-point mesh and keeping only the four bottom layers fixed to their bulk positions. Total energies reported throughout this manuscript were converged better than 10^{-5} eV in the self-consistent field, and geometries were relaxed until the energy threshold of 10^{-4} eV was fulfilled. Spin-polarized calculations were carried out when needed, and a careful analysis of all the possible open-shell spin states was performed (Table S1).

To locate transition states, we used the Improved Dimer Method[40] (IDM) and the Climbing Image Nudged Elastic Band[41] (CI-NEB) algorithms. For the latter, at least five images along the reaction coordinate were employed. The nature of all stationary points was confirmed by performing frequency

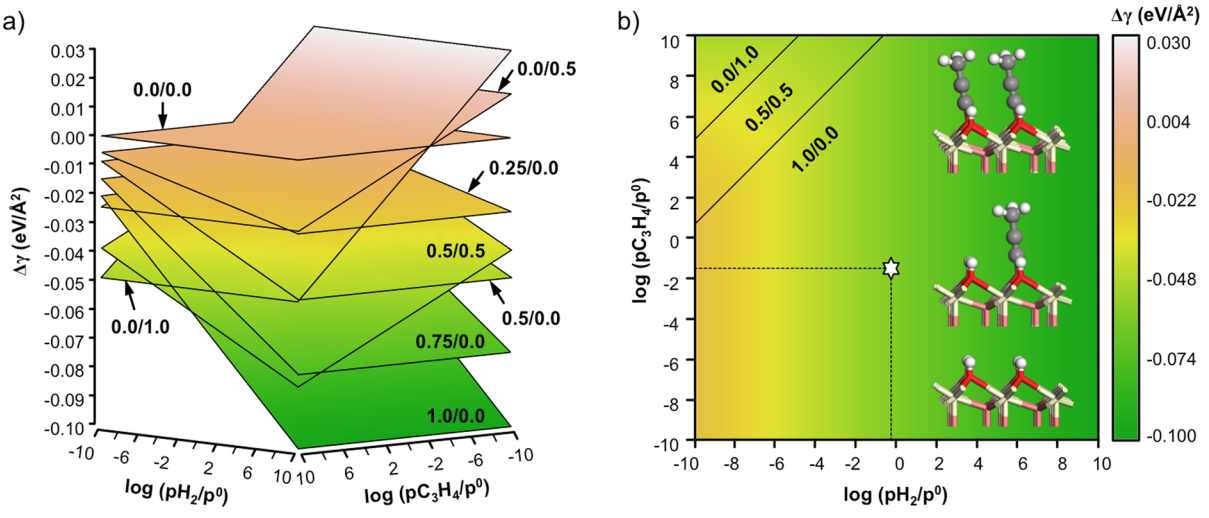

Figure 1. Tridimensional (a) and bidimensional perspectives (b) of the relative free energy surface of CeO_2(111) as a function of the H_2 and C_3H_4 pressures at the experimental reaction temperature, T = 523 K. Free energies are calculated taking the clean CeO_2(111) surface and the H_2 and C_3H_4 gas molecules as reference (see Supporting Information for details). A star marks the region corresponding to the optimal pressures reported in experiments. Insets of the most representative surfaces are also shown. Color code: Ce (pale yellow), surface O (red), subsurface O (pale red), C (silver), and H (white).

analysis with a numerical Hessian matrix obtained by atomic displacements of 0.02 Å.

For the most relevant steps, the PBE+*U* methodology was benchmarked against the HSE06 hybrid functional.[42] As these calculations are much more time-consuming, they were performed with a reduced cutoff of 400 eV and at the Γ−point. The HSE06 results presented in Table S2 confirm the good performance (within 0.15 eV) of the PBE+*U* methodology for this catalytic system.

3. RESULTS AND DISCUSSION

The reported strong dependence of propene selectivity on the hydrogen/propyne feed[21] suggests that hydrogenation on CeO_2 is severely affected by the surface coverage. Hence, we first investigated the $CeO_2(111)$ surface termination as a function of the H_2 and C_3H_4 gas phase reservoirs. To this aim, we explored the most representative configurations that might result from the interaction of those gases with CeO_2, and we analyzed them by means of ab initio thermodynamics.[43]

Although impeded by a sizable barrier of 1.08 eV, H_2 dissociates on CeO_2 leading to the hydroxylation of the surface and releasing more than 2 eV/molecule.[24] Thus, we considered several H coverages ranging from 0.25 to 1.0 ML as the most likely configurations resulting from that interaction. Similarly, calculations on the homolytic dissociation of propyne to form O−H and O−$CCCH_3$ surface terminations revealed that this is an exothermic process by 1.7 eV/molecule. Conversely, the heterolytic dissociation leading to an O−H and Ce−$CCCH_3$ coverage was found to be endothermic by 0.43 eV. Therefore, only coverages of the homolytically dissociated C_3H_4 were selected as representative configurations for the interaction of this gas with CeO_2. In particular, we examined the coverages corresponding to the dissociation of one and two C_3H_4 molecules, 0.5 and 1.0 ML, respectively.

In order to account for the interaction of both gases with CeO_2, a mixed coverage of 0.5 ML of H and 0.5 ML of C_3H_4 was also considered. It should be noted that in all the selected surfaces, the electrons from the cleaved sigma bonds are transferred directly to the lattice, which causes the partial reduction of the metal ions from Ce^{4+} to Ce^{3+}. For these configurations, we calculated all the possible open-shell spin states (Table S1) and found that all these states are (almost) degenerate. This was also noted by Ganduglia-Pirovano et al.[44] and in other works cited therein. The results derived from the ab initio thermodynamics on all these structures are summarized in the three-dimensional plot presented in Figure 1a. In this graphic, the most likely coverage at the given H_2 and C_3H_4 partial pressures and the reaction temperature of 523 K corresponds to that with the lowest relative free energy surface, $\Delta\gamma$. This can be more easily identified by inspecting the two-dimensional projection shown in Figure 1b.

According to the relative free surface energies reported in Figure 1, up to three different coverages might exist within the range of the considered pressures. More specifically, for very low H_2/C_3H_4 ratios, the full coverage of the homolytically dissociated C_3H_4 (0.0/1.0 ML) is the most likely, whereas for low ratios, a mixed coverage of H and C_3H_4 (0.5/0.5 ML) is expected. On the other hand, Figure 1 suggests that, from relatively high to very high H_2/C_3H_4 ratios, a fully hydroxylated surface (1.0/0.0 ML) with all the Ce atoms reduced prevails (Figure S1). This termination spreads across a wide range of gas pressures, including those used in experiments.[21] We used this surface coverage, corresponding to the resting state, as the starting point for our investigation of the operative hydrogenation mechanism.

It is important to note that, with the CeO_2 catalyst completely hydroxylated, only the acidic Ce sites from the surface are accessible for further reactivity. This resting state not only reduces the number of potential mechanisms for hydrogenation but also implies that propyne (or hydrogen) can only adsorb on top of the Ce^{3+} ions. This high surface occupation blocks the adsorption of adjacent alkynes and limits its diffusion, thus avoiding the formation of oligomers and leaving overhydrogenation as the only selectivity-compromising route.

The interaction between C_3H_4 and the resting state of CeO_2 is rather weak, as the binding energy lower than 0.10 eV demonstrates. Test calculations indicate that the inclusion of vdW interactions stabilizes adsorbates by ∼0.1 eV. These contributions, however, may affect all the other species involved in the reaction mechanism by a rather constant amount, and thus they do not affect the present conclusions. Similarly, H_2 can also molecularly adsorb on a neighboring Ce^{3+} center. In this case, however, the H_2−CeO_2 interaction is even less exothermic than that with C_3H_4, which explains why a large H_2/C_3H_4 feed is required in the optimal reaction conditions. Interestingly, the proximity of the two adsorbed gases in this structure suggests the simultaneous addition of H_2 to C_3H_4 (Scheme 1) as a plausible hydrogenation mechanism. In fact, two variants of this concerted path can be envisaged (Scheme 2). The first one involves the concurrent transfer of the two

Scheme 2. Schematic Representation of the (a) Four- and (b) Six-Membered Ring Transition States Proposed for the Semi-Hydrogenation of Propyne

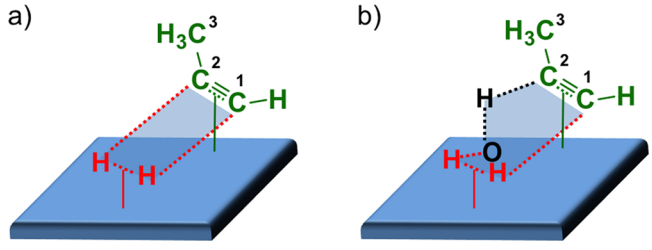

hydrogens in H_2 via a cyclic transition state constituted by these atoms and the C_1 and C_2 from C_3H_4 (Scheme 2a). This transition state structure was located and is presented in Figure 2. The optimized structure features a much shorter C_1−H distance compared to the C_2−H one, and a rather elongated H−H bond. Thus, this concerted step can be considered as a nonsynchronous-like process according to the different extension of C−H bond formation. To gain a deeper insight into the reactivity within this transition state, we calculated the charge density difference in this species, as shown in Figure 2. According to this representation, the H nearest to the C_1 is transferred as a hydride, whereas the second H is added to the C_2 as a proton. Unfortunately, the calculated energy for this transition state, 3.43 eV, is too high to be operative at the experimental temperature of 523 K.

The second concerted pathway consists in incorporating one H atom from the adsorbed H_2 and one H atom from a nearby O−H lattice to the organic moiety (Scheme 2b). Thus, the transition state associated with this mechanism corresponds to a six-membered ring structure that includes the adsorbed H_2, the C_1 and C_2 from C_3H_4, and an O−H group from the surface.

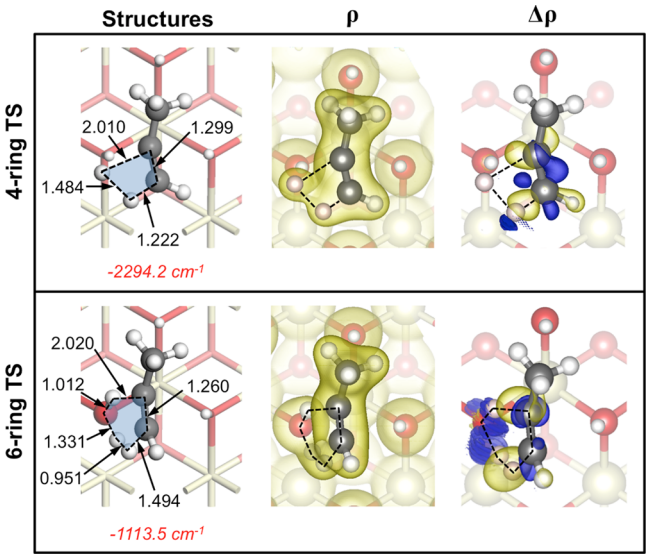

Figure 2. Top views of the optimized structures, total charge density, charge density difference, and imaginary frequencies (in red) for the four- and six-membered ring transition states. The charge density difference was calculated with respect to the isolated H_2, C_3H_4, and CeO_2 fragments at the transition state geometries. Yellow (blue) isosurfaces indicate accumulation (depletion) of the charge density.

This transition state structure was also located and is shown in Figure 2. As in the above four-membered structure, the representation of the charge density difference in this species clearly indicates that the closest H to the C_1 is added as a hydride. However, in this case, the other H atom in H_2 coordinates to a nearby O−H lattice at the same time that the proton from this group is abstracted by the C_2. The calculated energy for this nonsynchronous transition state, corrected by the zero-point vibrational energy, is 1.88 eV. This value is significantly lower than that for the four-membered ring transition state, which makes this pathway plausible under the experimental conditions. It is worth mentioning that the entropic requirements of the concerted transition state are abated by both the high H-coverage on the surface that limits the possible interactions of the incoming H_2 molecules and the strong templating effect of the surface ensembles that leads to the formation of a six-membered ring transition state. Furthermore, this energy is ∼1 eV lower than the one reported earlier for the semihydrogenation of acetylene and based on a Horiuti−Polanyi-like mechanism.[22] This difference at the experimental temperature of 523 K represents a rate increase of more than 9 orders of magnitude, confirming the only operation of the concerted hydrogenation mechanism.

To shed light on the preeminence of the six-membered transition state over the four-membered one, we next performed an activation-strain analysis on these two structures (Table S3).[45] In this type of analysis, the transition state energies are decomposed as $E_{TS} = E_{dist} + E_{int}$, where E_{dist} and E_{int} are the distortion and interaction energies, respectively. The E_{dist} can be understood as the energy cost associated with the geometric distortion of the CeO_2, H_2 and C_3H_4 fragments from their structure as isolated species to their "strained" geometries in the transition state. On the other hand, E_{int} stands for the energy gain arising from the interaction of those fragments with each other in the transition state. Interestingly, the calculated E_{dist} terms were found to be rather similar for the two cyclic structures, with the CeO_2 fragment exhibiting the highest energy difference in favor of the four-membered structure ($|\Delta E_{dist}| \approx 0.15$ eV). This can be rationalized with the fact that the six-membered transition state involves an O−H group from the CeO_2 surface, and therefore, the geometric distortion of this fragment requires a higher energy. Nevertheless, the largest difference between the two transition states resulted to be in the E_{int} term ($|\Delta E_{int}| \approx 4$ eV), which indicates that the preeminence of the six-membered geometry mainly originates from the templating surface effects.

Overall, the results presented so far provide firm theoretical evidence that the partial hydrogenation of propyne on CeO_2 occurs through the concerted mechanism summarized in Figure 3. It starts with a completely hydroxylated $CeO_2(111)$ surface,

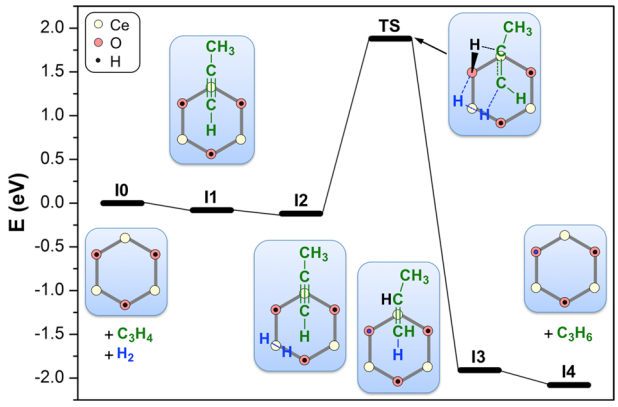

Figure 3. Overall reaction energy profile for the selective hydrogenation of propyne. For the sake of clarity, the fully hydroxylated $CeO_2(111)$ surface is represented by a gray hexagon, where the Ce, O, and H surface atoms are depicted as pale yellow, red, and black spheres, respectively. The energy of **TS** has been corrected by the ZPVE.

followed by the sequential adsorption of C_3H_4 and H_2 on top of two surface Ce^{3+} ions that leads to **I1** and **I2**, respectively. Then, **I2** undergoes concerted hydrogenation of the adsorbed C_3H_4 via a six-membered ring transition state (**TS**). This step results in **I3**, from which the alkene readily desorbs in an exothermic process. The highest energy point in the overall energy profile corresponds to **TS**. Therefore, the concerted addition of the two H atoms to the alkyne is the rate-determining step.

For completeness, we also investigated the subsequent (over)hydrogenation of propene to propane, see Supporting Information. In this case, the presence of two additional H atoms in the adsorbed alkene frustrates a concerted transition state and causes the reaction to occur in two steps: first, the H from the surface OH group is transferred to the C_2 of the olefin, and then, the adsorbed H_2 dissociates heterolytically regenerating the surface OH and yielding the final alkane. The first step is the most energy demanding with an energy barrier of 2.69 eV. This energy is significantly higher than the 1.88 eV required for the hydrogenation of propyne to propene, which explains the excellent selectivities obtained in experiments by kinetic arguments. Importantly, the energy of the transition state associated with the overhydrogenation of propene, 2.69 eV, is even lower than that reported for the hydrogenation of acetylene to ethylene via a Horiuti−Polanyi mechanism, 2.86 eV.[22]

The concerted mechanism presented in Figure 3 also accounts for the rest of experimental observations.[21] For

example, the increasing alkene selectivity with the H_2/C_3H_4 ratio can be attributed to the full H coverage that prevents the adsorption of alkyne molecules in adjacent positions and hinders its diffusion along the surface avoiding the formation of byproducts by oligomerization. The detrimental effect of oxygen vacancies on the catalytic activity can be also explained by the reduction of the number of active sites, as surface O atoms have been shown to play an active role in the hydrogenation transition state. Hence, a reduced catalytic activity should be expected when increasing the number of oxygen vacancies (e.g., by doping the CeO_2 surface).[46] Besides, the concerted mechanism ensures a unique *syn*-stereoselectivity, in agreement with the experiments,[21,22,47] and the delicate ensemble requirements might explain the recently reported structure sensitivity.[32]

4. CONCLUSIONS

In summary, the DFT calculations reported in this work show that the resting state of the CeO_2 catalyst in the semi-hydrogenation of propyne is decisive to understand its outstanding activity and sharp selectivity. We found that it corresponds to a fully hydroxylated and fully reduced surface, where the adsorbed H atoms play a two-fold role: they act as a hydrogen source for hydrogenation and further prevent the formation of oligomers by limiting the adsorption and diffusion of alkyne molecules. The full H coverage opens the way for an unprecedented concerted hydrogenation mechanism. The energy barrier for this path is about 1 eV lower than the Horiuti−Polanyi mechanism previously proposed for the hydrogenation of acetylene on CeO_2, and only leads to the *syn*-product in agreement with experiments. Therefore, the appearance of concerted pathways should be considered in future mechanistic studies on surfaces. This finding increases the list of hydrogenation paths and, accordingly, broadens the possibilities in the future design of more efficient and economic catalysts.

Finally, we would like to point out that the preeminence of Density Functional Theory to unravel complex mechanisms is further reinforced by the fact that even kinetic data, typically employed to determine reaction orders and afterward infer the mechanism,[10] might not be conclusive. Our kinetic analysis, see Supporting Information, indicates that both H_2 and C_3H_4 reaction orders for the concerted hydrogenation mechanism should lay between −1 and 1, and thus, partially overlap with the values for a Horiuti-Polanyi mechanism, which does not allow further mechanistic considerations.

■ ASSOCIATED CONTENT

Supporting Information

Details on the ab initio thermodynamics, energies of the surface configurations with different open-shell spin states, benchmark calculations with the HSE06 hybrid functional, spin densities on the surface Ce^{3+} ions of the CeO_2 resting state structure, activation-strain analysis, fractional coordinates for the four and six-membered ring transition states, derived kinetic equations, and optimized structure for the highest energy transition state involved in the (over)hydrogenation of propene.

■ AUTHOR INFORMATION

Corresponding Author

*E-mail: maxgarcia@iciq.es, maxg@slac.stanford.edu. Fax: (+34) 977920231. Tel: (+34) 977920200.

Notes

The authors declare no competing financial interest.

■ ACKNOWLEDGMENTS

We thank EU (ERC-2010-StG-258406) and MINECO (CTQ2012-33826/BQU) for financial support and BSC-RES for providing generous access to their computational resources. We also thank Moisés Álvarez Moreno for technical support.

■ REFERENCES

(1) Abild-Pedersen, F.; Greeley, J.; Studt, F.; Rossmeisl, J.; Munter, T. R.; Moses, P. G.; Skúlason, E.; Bligaard, T.; Nørskov, J. K. *Phys. Rev. Lett.* **2007**, *99*, 016105.

(2) Nørskov, J. K.; Bligaard, T.; Rossmeisl, J.; Christensen, C. H. *Nat. Chem.* **2009**, *1*, 37−46.

(3) Derrien, M. L. In *Catalytic Hydrogenation*; Červený, L., Ed.; Elsevier: Amsterdam, 1986; Vol. *27*, pp 613−666.

(4) Bond, G. C. *Metal-Catalysed Reactions of Hydrocarbons*; Springer: New York, 2005; Vol. *21*, pp 395−436.

(5) Borodziński, A.; Bond, G. C. *Catal. Rev.* **2006**, *48*, 91−144.

(6) Borodziński, A.; Bond, G. C. *Catal. Rev.* **2008**, *50*, 379−469.

(7) Arnold, H.; Döbert, F.; Gaube, J. In *Handbook of Heterogeneous Catalysis*; Wiley-VCH Verlag GmbH & Co. KGaA: Weinheim, 2008; pp 3266−3284.

(8) Crespo-Quesada, M.; Cárdenas-Lizana, F.; Dessimoz, A.-L.; Kiwi-Minsker, L. *ACS Catal.* **2012**, *2*, 1773−1786.

(9) Mitsudome, T.; Kaneda, K. *Green Chem.* **2013**, *15*, 2636−2654.

(10) Vilé, G.; Baudouin, D.; Remediakis, I. N.; Copéret, C.; López, N.; Pérez-Ramírez, J. *ChemCatChem* **2013**, *5*, 3750−3759.

(11) Teschner, D.; Borsodi, J.; Wootsch, A.; Révay, Z.; Hävecker, M.; Knop-Gericke, A.; Jackson, S. D.; Schlögl, R. *Science* **2008**, *320*, 86−89.

(12) Teschner, D.; Révay, Z.; Borsodi, J.; Hävecker, M.; Knop-Gericke, A.; Schlögl, R.; Milroy, D.; Jackson, S. D.; Torres, D.; Sautet, P. *Angew. Chem., Int. Ed.* **2008**, *47*, 9274−9278.

(13) Teschner, D.; Borsodi, J.; Kis, Z.; Szentmiklósi, L.; Révay, Z.; Knop-Gericke, A.; Schlögl, R.; Torres, D.; Sautet, P. *J. Phys. Chem. C* **2010**, *114*, 2293−2299.

(14) Studt, F.; Abild-Pedersen, F.; Bligaard, T.; Sørensen, R. Z.; Christensen, C. H.; Nørskov, J. K. *Angew. Chem., Int. Ed.* **2008**, *47*, 9299−9302.

(15) Armbrüster, M.; Behrens, M.; Cinquini, F.; Föttinger, K.; Grin, Y.; Haghofer, A.; Klötzer, B.; Knop-Gericke, A.; Lorenz, H.; Ota, A.; Penner, S.; Prinz, J.; Rameshan, C.; Révay, Z.; Rosenthal, D.; Rupprechter, G.; Sautet, P.; Schlögl, R.; Shao, L.; Szentmiklósi, L.; Teschner, D.; Torres, D.; Wagner, R.; Widmer, R.; Wowsnick, G. *ChemCatChem* **2012**, *4*, 1048−1063.

(16) Molnár, Á.; Sárkány, A.; Varga, M. *J. Mol. Catal. A* **2001**, *173*, 185−221.

(17) Vilé, G.; Almora-Barrios, N.; Mitchell, S.; López, N.; Pérez-Ramírez, J. *Chem.—Eur. J.* **2014**, *20*, 5926−5937.

(18) García-Mota, M.; Bridier, B.; Pérez-Ramírez, J.; López, N. *J. Catal.* **2010**, *273*, 92−102.

(19) Armbrüster, M.; Kovnir, K.; Friedrich, M.; Teschner, D.; Wowsnick, G.; Hahne, M.; Gille, P.; Szentmiklósi, L.; Feuerbacher, M.; Heggen, M.; Girgsdies, F.; Rosenthal, D.; Schlögl, R.; Grin, Y. *Nat. Mater.* **2012**, *11*, 690−693.

(20) Studt, F.; Abild-Pedersen, F.; Bligaard, T.; Sørensen, R. Z.; Christensen, C. H.; Nørskov, J. K. *Science* **2008**, *320*, 1320−1322.

(21) Vilé, G.; Bridier, B.; Wichert, J.; Pérez-Ramírez, J. *Angew. Chem., Int. Ed.* **2012**, *51*, 8620−8623.

(22) Carrasco, J.; Vilé, G.; Fernández-Torre, D.; Pérez, R.; Pérez-Ramírez, J.; Ganduglia-Pirovano, M. V. *J. Phys. Chem. C* **2014**, *118*, 5352−5360.

(23) We noted that this statement, made by the authors of ref 22, is not consistent with the energy barriers reported therein, as the most energy demanding step corresponds to the addition of the second H atom to the organic moiety (2.86 eV) and not the initial H_2 dissociation (1.00 eV).

(24) García-Melchor, M.; López, N. *J. Phys. Chem. C* **2014**, *118*, 10921−10926.
(25) Metiu, H.; Chrétien, S.; Hu, Z.; Li, B.; Sun, X. *J. Phys. Chem. C* **2012**, *116*, 10439−10450.
(26) Horiuti, I.; Polanyi, M. *Trans. Faraday Soc.* **1934**, *30*, 1164−1172.
(27) Mei, D.; Sheth, P. A.; Neurock, M.; Smith, C. M. *J. Catal.* **2006**, *242*, 1−15.
(28) Bridier, B.; López, N.; Peréz-Ramírez, J. *Dalton Trans.* **2010**, *39*, 8412−8419.
(29) Segura, Y.; López, N.; Pérez-Ramírez, J. *J. Catal.* **2007**, *247*, 383−386.
(30) Macomber, R. S. *Organic Chemistry Vol. II: Chemical Behavior of Organic Compounds and Multi-step Organic Synthesis*; University Science Books: Mill Valley, CA, 1996; pp 58−103.
(31) Sankararaman, S. *Pericyclic Reactions: A Textbook: Reactions, Applications and Theory*; Wiley-VCH: London, 2005; pp 1−432.
(32) Vilé, G.; Colussi, S.; Krumeich, F.; Trovarelli, A.; Pérez-Ramírez, J. *Angew. Chem., Int. Ed.* **2014**, DOI: 10.1002/anie.201406637.
(33) Kresse, G.; Furthmüller, J. *Phys. Rev. B* **1996**, *54*, 11169−11186.
(34) Kresse, G.; Furthmüller, J. *Comput. Mater. Sci.* **1996**, *6*, 15−50.
(35) Blöchl, P. E. *Phys. Rev. B* **1994**, *50*, 17953−17979.
(36) Perdew, J. P.; Burke, K.; Ernzerhof, M. *Phys. Rev. Lett.* **1996**, *77*, 3865−3868.
(37) Dudarev, S. L.; Botton, G. A.; Savrasov, S. Y.; Humphreys, C. J.; Sutton, A. P. *Phys. Rev. B* **1998**, *57*, 1505−1509.
(38) Fabris, S.; de Gironcoli, S.; Baroni, S.; Vicario, G.; Balducci, G. *Phys. Rev. B* **2005**, *71*, 041102−4.
(39) Kümmerle, E. A.; Heger, G. *J. Solid State Chem.* **1999**, *147*, 485−500.
(40) Heyden, A.; Bell, A. T.; Keil, F. J. *J. Chem. Phys.* **2005**, *123*, 224101.
(41) Henkelman, G.; Uberuaga, B. P.; Jónsson, H. *J. Chem. Phys.* **2000**, *113*, 9901−9904.
(42) Krukau, A. V.; Vydrov, O. A.; Izmaylov, A. F.; Scuseria, G. E. *J. Chem. Phys.* **2006**, *125*, 224106.
(43) Wang, X.-G.; Chaka, A.; Scheffler, M. *Phys. Rev. Lett.* **2000**, *84*, 3650−3653.
(44) Ganduglia-Pirovano, M. V.; Da Silva, J. L. F.; Sauer, J. *Phys. Rev. Lett.* **2009**, *102*, 026101.
(45) For an example of this type of analysis see: García-Melchor, M.; Gorelsky, S. I.; Woo, T. K. *Chem.—Eur. J.* **2011**, *17*, 13847−13853 and references therein..
(46) Farra, R.; García-Melchor, M.; Eichelbaum, M.; Hashagen, M.; Frandsen, W.; Allan, J.; Girgsdies, F.; Szentmiklósi, L.; López, N.; Teschner, D. *ACS Catal.* **2013**, *3*, 2256−2268.
(47) Vilé, G.; Wrabetz, S.; Floryan, L.; Schuster, M. E.; Girgsdies, F.; Teschner, D.; Pérez-Ramírez, J. *ChemCatChem* **2014**, *6*, 1928−1934.